Article (refereed) - postprint

Bloschl, Gunter; Hall, Julia; Parajka, Juraj; Perdigao, Rui A.P.; Merz, Bruno; Arheimer, Berit; Aronica, Giuseppe T.; Bilibashi, Ardian; Bonacci, Ognjen; Borga, Marco; Canjevac, Ivan; Castellarin, Attilio; Chirico, Giovanni B.; Claps, Pierluigi; Fiala, Karoly; Frolova, Natalia; Gorbochova, Liudmyla; Gul, Ali; **Hannaford, Jamie**; **Harrigan, Shaun**; Kireeva, Maria; Kiss, Andrea; Kjeldsen, Thomas R.; Khonova, Silvia; Koskela, Jarkko J.; Ledvinka, Ondrej; Macdonald, Neil; Mavrova-Guirguinova, Maria; Mediero, Luis; Merz, Ralf; Molnar, Peter; Montanari, Alberto; Murphy, Conor; Osuch, Marzena; Ovcharuk, Valeryia; Radevski, Ivan; Rogger, Magdalena; Salinas, Jose L.; Sauquet, Eric; Sraj, Mojca; Szolgay, Jan; Viglione, Alberto; Volpi, Elena; Wilson, Donna; Zaimi, Klodian; Zivkovic, Nenad. 2017. **Changing climate shifts timing of European floods.** *Science*, 357 (6351). 588-590. https://doi.org/10.1126/science.aan2506

Title: Changing climate shifts timing of European floods

Authors:

Günter Blöschl[1*], Julia Hall[1], Juraj Parajka[1], Rui A. P. Perdigão[1], Bruno Merz[2], Berit Arheimer[3], Giuseppe T. Aronica[4], Ardian Bilibashi[5], Ognjen Bonacci[6], Marco Borga[7], Ivan Čanjevac[8], Attilio Castellarin[9], Giovanni B. Chirico[10], Pierluigi Claps[11], Károly Fiala[12], Natalia Frolova[13], Liudmyla Gorbachova[14], Ali Gül[15], Jamie Hannaford[16], Shaun Harrigan[16], Maria Kireeva[13], Andrea Kiss[1], Thomas R. Kjeldsen[17], Silvia Kohnová[18], Jarkko J. Koskela[19], Ondrej Ledvinka[20], Neil Macdonald[21], Maria Mavrova-Guirguinova[22], Luis Mediero[23], Ralf Merz[24], Peter Molnar[25], Alberto Montanari[9], Conor Murphy[26], Marzena Osuch[27], Valeryia Ovcharuk[28], Ivan Radevski[29], Magdalena Rogger[1], José L. Salinas[1], Eric Sauquet[30], Mojca Šraj[31], Jan Szolgay[18], Alberto Viglione[1], Elena Volpi[32], Donna Wilson[33], Klodian Zaimi[34], and Nenad Živković[35]

Affiliations:

[1]Institute of Hydraulic Engineering and Water Resources Management, Technische Universität Wien, Vienna, Austria.

[2]Helmholtz Centre Potsdam, GFZ German Research Centre for Geosciences, Potsdam, Germany.

[3]Swedish Meteorological and Hydrological Institute, Norrköping, Sweden.

[4]Department of Engineering, University of Messina, Messina, Italy.

[5]CSE – Control Systems Engineer, Renewable Energy Systems & Technology, Tirana, Albania.

[6]Faculty of Civil Engineering, Architecture and Geodesy, Split University, Split, Croatia.

[7]Department of Land, Environment, Agriculture and Forestry, University of Padova, Padua, Italy.

[8]University of Zagreb, Faculty of Science, Department of Geography, Zagreb, Croatia.

[9]Department of Civil, Chemical, Environmental and Materials Engineering (DICAM), Università di Bologna, Bologna, Italy.

[10]Department of Agricultural Sciences, University of Naples Federico II, Naples, Italy.

[11]Department Environment, Land and Infrastructure Engineering (DIATI), Politecnico di Torino, Turin, Italy.

[12]Lower Tisza District Water Directorate, Szeged, Hungary.

[13]Department of Land Hydrology, Lomonosov Moscow State University, Moscow, Russia.

[14]Department of Hydrological Research, Ukrainian Hydrometeorological Institute, Kiev, Ukraine.

[15]Department of Civil Engineering, Dokuz Eylul University, Izmir, Turkey.

[16]Centre for Ecology & Hydrology, Wallingford, Oxfordshire, UK.

[17]Department of Architecture and Civil Engineering, University of Bath, Bath, UK.

[18]Slovak University of Technology in Bratislava, Faculty of Civil Engineering, Department of Land and Water Resources Management, Radlinského 11, 810 05 Bratislava, Slovakia.

[19]Finnish Environment Institute, Helsinki, Finland.

[20]Czech Hydrometeorological Institute, Prague, Czechia.

[21]Department of Geography and Planning & Institute of Risk and Uncertainty, University of Liverpool, Liverpool, UK.

[22]University of Architecture, Civil Engineering and Geodesy, Sofia, Bulgaria.

[23]Department of Civil Engineering: Hydraulic, Energy and Environment, Technical University of Madrid, Madrid, Spain.

[24]Department for Catchment Hydrology, Helmholtz Centre for Environmental Research – UFZ, Halle, Germany.

[25]Institute of Environmental Engineering, ETH Zurich, Zurich, Switzerland.

[26] Irish Climate Analysis and Research Units (ICARUS), Department of Geography, Maynooth University, Ireland.

[27]Institute of Geophysics Polish Academy of Sciences, Department of Hydrology and Hydrodynamics, Warsaw, Poland.

[28]Hydrometeorological Institute, Odessa State Environmental University, Odessa, Ukraine.

[29]Institute of Geography, Faculty of Natural Sciences and Mathematics, Ss. Cyril and Methodius University, Skopje, Republic of Macedonia.

[30]Irstea, UR HHLY, Hydrology-Hydraulics Research Unit, Lyon, France.

[31]Faculty of Civil and Geodetic Engineering, University of Ljubljana, Ljubljana, Slovenia.

[32]Department of Engineering, University Roma Tre, Rome, Italy.

[33]Norwegian Water Resources and Energy Directorate, Oslo, Norway.

[34]Institute of Geo-Sciences, Energy, Water and Environment (IGEWE), Polytechnic University of Tirana, Tirana, Albania.

[35] University of Belgrade, Faculty of Geography, Belgrade, Serbia.

*Corresponding author. Email: bloeschl@hydro.tuwien.ac.at

Abstract:
A warming climate is expected to impact river floods; however, no consistent large-scale climate change signal in observed flood magnitudes has been identified so far. We have analyzed the timing of river floods in Europe over the last five decades using a pan-European database from 4262 observational hydrometric stations, and find clear patterns of change in flood timing. Warmer temperatures have led to earlier spring snowmelt floods throughout North-Eastern Europe; delayed winter storms associated with polar warming have led to later winter floods around the North Sea and some sectors of the Mediterranean Coast; and earlier soil moisture maxima have led to earlier winter floods in Western Europe. Our results highlight the existence of a clear climate signal in flood observations at the continental scale.

One Sentence Summary:
The observed timing of floods has shifted consistently in many parts of Europe over the past 50 years as a result of a changing climate.

Main Text:

River flooding affects more people worldwide than any other natural hazard, with an estimated global annual average loss of US $104 billion (1). Damages are expected to increase due to economic growth and climate change (2, 3). The intensification of the water cycle due to a warming climate is projected to change the magnitude, frequency and timing of river floods (3). However, existing studies have been unable to identify a consistent climate change signal in flood magnitudes (4). Identification of a large-scale climate change signal in flood observations has been hampered by the existence of many processes controlling floods, including precipitation, soil moisture and snow, by non-climatic drivers of flood change such as land use change and river training, and by the inconsistency of data sets and their limited spatial extents (4, 5). It has been proposed that considering the seasonal timing of floods as a fingerprint of climate effects on floods may be a way to avoid some of those complications (6, 7). For example, in cold regions, earlier snowmelt due to warmer temperatures leads to earlier spring floods (6), and this climate-related signal may be less confounded by non-climatic drivers than flood magnitudes themselves because of the strong seasonality of climate. While the changing timing of floods has been studied at local scale in Nordic and Baltic countries (8–10), no consistent analysis exists at the European scale.

Here we analyze a large data set of flood observations in Europe to assess whether a changing climate has shifted the timing of river floods in the last five decades. Our analysis is based on river discharge or water level observations from 4262 hydrometric stations in 38 European countries for the period 1960-2010 (Table S1). For each station, we use a series consisting of the dates of occurrence of the highest peak in any calendar year. We define the average timing of the floods by the average date on which floods have occurred during the

observation period. We then estimate the trend in the timing of the floods using the Theil-Sen slope estimator (11) for stations with at least 35 years of data and the long-term evolution using a 10-year moving average filter. Finally, we analyze the change signal of three potential drivers of flood changes in a similar fashion: the middle date of the maximum 7-day precipitation; the middle day of the month with the highest soil moisture; and the middle day of the first seven days in a year with air temperature above 0° C as a proxy for spring snowmelt and snowfall-to-rain transition. For more details on the data and the analysis see the Materials and Methods section in the Supplementary Material.

Our data show a clear shift in the timing of floods in Europe in the past 50 years (Fig. 1). The regionally interpolated trend patterns shown in Fig. 1, range from a –13 days per decade towards earlier floods to +9 days towards later floods, which translates into total shifts of –65 and +45 days, respectively, of linear trends over the entire 50 year period. The local, station specific, trends (Fig. S2) are larger, but reflect smaller scale rather than regional scale processes. The changes are most consistent in North-Eastern Europe (region 1 in Fig. 1) where 81% of the stations show a shift towards earlier floods (50% of the stations by more than –8 days / 50 yrs) (Fig. S2). The changes are largest in Western Europe along the North Atlantic Coast from Portugal to England (region 3) where 50% of the stations show a shift towards earlier floods by at least 15 days / 50 yrs (25% of the stations by more than 36 days / 50 yrs). Around the North Sea (region 2, South-Western Norway, the Netherlands, Denmark and Scotland) 50% of the stations show a shift towards later floods by more than 8 days / 50 yrs. In some parts of the Mediterranean Coast (region 4, North-Eastern Adriatic Coast, North-Eastern Spain), there is a shift towards later floods (50% of the stations by more than 5 days / 50 yrs). Apart from the

large-scale change patterns described for the four regions above, smaller-scale patterns of changes in flood timing can also be identified.

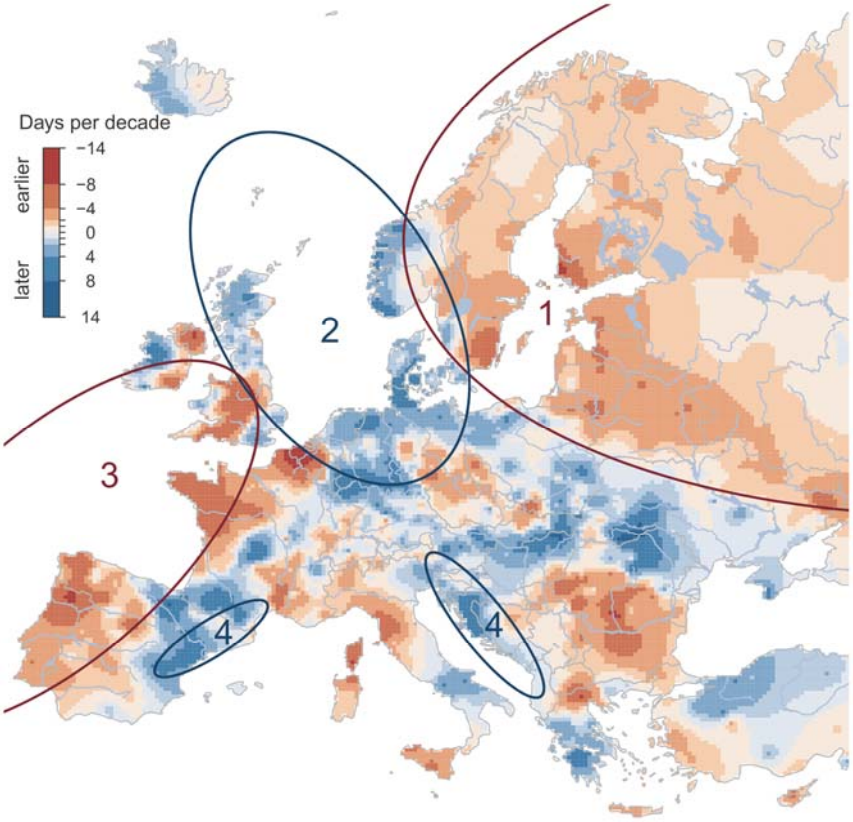

Fig. 1. Observed trends of river flood timing in Europe (1960-2010). Red indicates earlier floods, blue later floods (days per decade). 1-4 indicate regions with distinct drivers: [1] North-Eastern Europe: earlier snowmelt; [2] North Sea region: later winter storms; [3] Western Europe along the Atlantic Coast: earlier soil moisture maximum; [4] parts of the Mediterranean Coast: stronger Atlantic influence in winter.

In order to infer the causes of these changes in timing, we focused on six sub-regions or hotspots, where changes in flood timing are particularly clear (Fig. S2, Table S2). Since floods are the result of the seasonal interplay of precipitation, soil moisture and snow processes (12) we analyzed the temporal evolutions of these variables and compared them to those of the floods (Fig. 2A-2F). In Southern Sweden (Fig. 2A) and in the Baltics (Fig. 2B), floods are mainly due

77 to spring snowmelt (9, 10). The temporal evolution of flood timing therefore closely follows that
78 of snowmelt, shifting from late March to February (green and orange lines in Fig. 2A, 2B).
79 Earlier snowmelt is known to be driven by both local temperature increases and a decreasing
80 frequency of advection of arctic air masses (13). The Baltics are topographically less shielded
81 from these air masses than Southern Sweden, which is reflected by larger variations in the timing
82 of snowmelt in the 1990s. In South-Western Norway (Fig. 2C) precipitation maxima at the end
83 of the year generate floods around the same time, since there is little subsurface water storage
84 capacity there due to the prevalence of shallow soils. Changes in the North Atlantic Oscillation
85 (NAO) since 1980 (14) may have resulted in a delayed arrival of heavy winter precipitation, with
86 maxima shifting from October to December. These NAO anomalies have been less pronounced
87 since the early 2000s. The floods follow closely the timing of extreme precipitation (Fig. 2C),
88 which strongly suggests a causal link. The changes in the NAO may be related to Polar warming,
89 among many other factors, although the role of anthropogenic effects is still uncertain (15, 16).
90 In Southern England (Fig. 2D), the subsurface water storage capacity tends to be much larger
91 than in coastal Norway. The maximum rainfall, which occurs in autumn, therefore tends to get
92 stored, and soil moisture and groundwater tables continuously increase until they reach a
93 maximum in winter. Sustained winter rainfall on saturated soils then produces the largest floods
94 in winter. As a result, the flood timing in Southern England is more closely associated with the
95 timing of maximum soil moisture than with the timing of extreme precipitation (17). The
96 variations in flood timing in North-Western Iberia (Fig. 2E) are similar to those of Southern
97 England, although precipitation there occurs more in the winter, so extreme precipitation and
98 maximum soil moisture (driven by sustained precipitation) are more closely aligned. Along the
99 Northern Adriatic Coast (Fig. 2F), large-scale influences by the Atlantic Ocean condition

Adriatic meso-scale cyclonic activity, which produces heavy precipitation towards the end of the year (18). Meridional shifts in storm tracks have increased atmospheric flow from the Atlantic to the Mediterranean in winter (19), leading to later extreme precipitation and floods in the season (Fig. 2F).

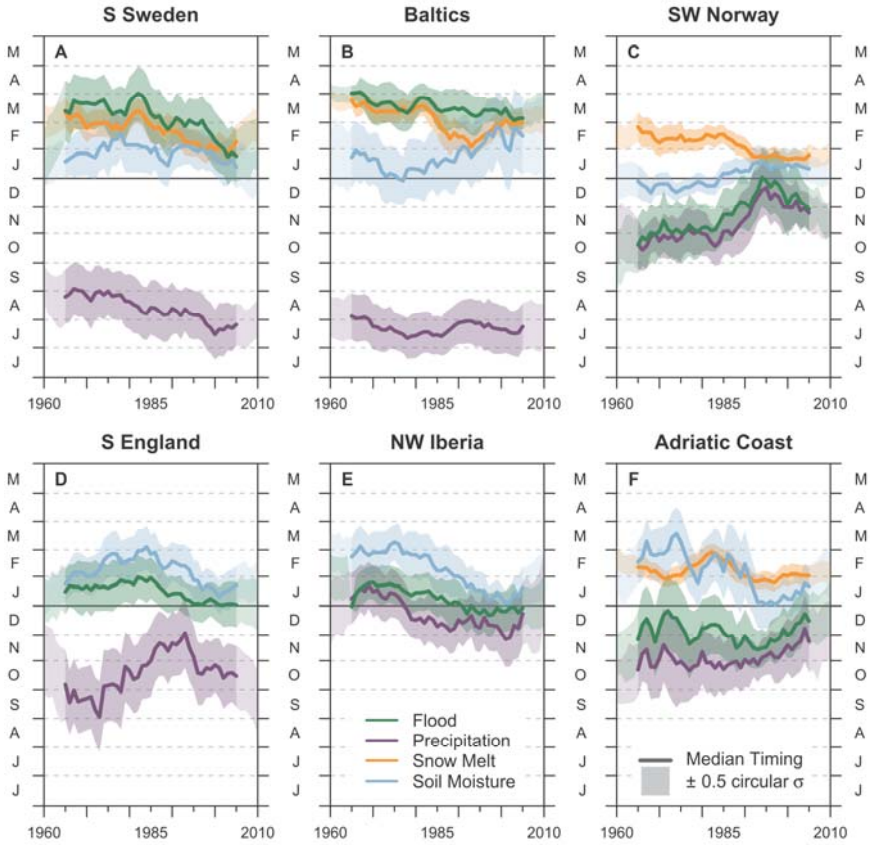

Fig. 2. Long-term temporal evolution of timing of floods and their drivers for six hotspots in Europe. Southern Sweden (**A**), Baltics (**B**), South-Western Norway (**C**), Southern England (**D**), North-Western Iberia (**E**), Adriatic Coast (**F**). Timing of observed floods (green), 7-day maximum precipitation (purple), snowmelt indicator (orange), and timing of modeled maximum soil moisture (blue). Line shows median timing over the entire hotspot, bands indicate variability of timing within the year (± 0.5 circular standard deviation (Eq. 8)). All data were subject to a 10-year moving average filter. Vertical axes show month of the year (June to May).

113 To further assist in the interpretation of trends in flood timing across Europe, the spatial
114 pattern of the average flood timing (1960-2010) is presented in Fig. 3. The average timing of the
115 floods varies gradually from the West to the East due to increasing continentality (distance from
116 the Atlantic), and from the South to the North due to the increasing influence of snow processes.
117 The effect of snow storage and melt at high altitudes, e.g. in the Alps and the Carpathians (red
118 arrows in Fig. 3), is superimposed on this pattern. The spatial patterns of the average timing of
119 potential drivers, and their trends, are shown in Fig. S3, S4, S5.

120 Throughout North-Eastern Europe (region 1 in Fig. 1), spring occurrence of snowmelt and
121 floods (yellow and green arrows in Fig. S4A and Fig. S3) combined with a warmer climate (Fig.
122 S4A) has led to earlier floods. In the region around the North Sea (region 2 in Fig. 1), extreme
123 precipitation and floods in the winter (blue arrows in Fig. S3A and Fig. 3) combined with a shift
124 in the timing of extreme winter precipitation (Fig. S3B) has led to later floods. In Western
125 Europe (region 3 in Fig. 1), winter occurrence of soil moisture maxima and floods (blue arrows
126 in Fig. S5A and Fig. 3) combined with a shift in the timing of soil moisture maxima (Fig. S5B)
127 has led to earlier floods. While region 3 shows a consistent behavior in flood timing changes,
128 closely aligned with those of soil moisture, the effect of changing storm tracks on precipitation
129 are different in Southern England and North-Western Iberia, due to the opposite effects of the
130 NAO.

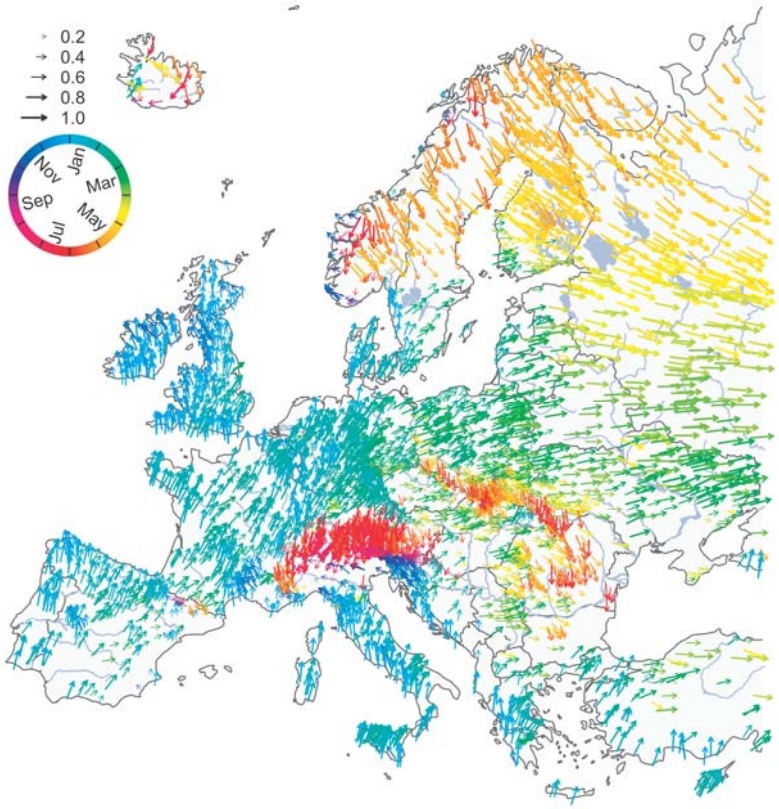

Fig. 3. Observed average timing of river floods in Europe (1960-2010). Each arrow represents one hydrometric station (n=4062). Color and arrow direction indicate the average timing of floods (light blue: winter floods (DJF), green to yellow: spring floods (MAM), orange to red summer floods (JJA) and purple to dark blue autumn floods (SON)). Lengths of the arrows indicate the concentration of floods within a year (R=0 evenly distributed, R=1 all floods occur on the same date).

If the trends in flood timing continue, considerable economic and environmental consequences may arise, as society and ecosystems have adapted to the average within-year timing of floods. Later winter floods in catchments around the North Sea, for example, may reduce agricultural productivity due to softer ground for spring farming operations, higher soil compaction, enhanced erosion and direct crop damage (20). Spring floods occurring earlier in the season in North-Eastern Europe may limit the replenishment of reservoirs if managers expect later floods that never arrive, with substantial reductions in water supply, irrigation and

hydropower generation (21). Perhaps more importantly, this study identifies a clear climate change signal in flood observations at the continental scale using the timing of floods, which was not possible using flood magnitudes to date (4, 5, 22).

References and Notes:

1. UNISDR, "Making Development Sustainable: The Future of Disaster Risk Management. Global Assessment Report on Disaster Risk Reduction" (Geneva, Switzerland: United Nations International Strategy for Disaster Reduction (UNISDR), 2015).

2. H. C. Winsemius *et al.*, Global drivers of future river flood risk. *Nat. Clim. Chang.* **6**, 381–385 (2016).

3. IPCC, *Managing the Risks of Extreme Events and Disasters to Advance Climate Change Adaptation. A Special Report of Working Groups I and II of the Intergovernmental Panel on Climate Change* (Cambridge University Press, Cambridge, UK and New York, NY, USA, 2012).

4. J. Hall *et al.*, Understanding flood regime changes in Europe: a state of the art assessment. *Hydrol. Earth Syst. Sc.* **18**, 2735–2772 (2014).

5. Z. Kundzewicz, *Changes in flood risk in Europe* (IAHS Press Wallingford, 2012).

6. J. Parajka *et al.*, Seasonal characteristics of flood regimes across the Alpine-Carpathian range. *J. Hydrol.* **394**, 78–89 (2010).

7. R. Merz, G. Blöschl, A process typology of regional floods. *Water Resour. Res.* **39**, 1340 (2003).

8. D. Wilson, H. Hisdal, D. Lawrence, Has streamflow changed in the Nordic countries? – Recent trends and comparisons to hydrological projections. *J. Hydrol.* **394**, 334–346 (2010).

9. B. Arheimer, G. Lindström, Climate impact on floods: changes in high flows in Sweden in the past and the future (1911–2100). *Hydrol. Earth Syst. Sc.* **19**, 771–784 (2015).

10. D. Sarauskiene, J. Kriauciuniene, A. Reihan, M. Klavins, Flood pattern changes in the rivers of the Baltic countries. *J. Environ. Eng. Landsc.* **23**, 28–38 (2015).

11. P. K. Sen, Estimates of the Regression Coefficient Based on Kendall's Tau. *J. Am. Stat. Assoc.* **63**, 1379–1389 (1968).

12. M. Sivapalan, G. Blöschl, R. Merz, D. Gutknecht, Linking flood frequency to long-term water balance: Incorporating effects of seasonality. *Water Resour. Res.* **41**, W06012 (2005).

13. A. Draveniece, Detecting changes in winter seasons in Latvia: the role of arctic air masses. *Boreal. Environ. Res.* **14**, 89–99 (2009).

14. J. W. Hurrell, H. Van Loon, Decadal variations in climate associated with the North Atlantic Oscillation. *Clim. Chang.* **36**, 301–326 (1997).

15. N. P. Gillett *et al.*, Attribution of polar warming to human influence. *Nat. Geosci.* **1**, 750–754 (2008).

16. E. Hanna, T. E. Cropper, P. D. Jones, A. A. Scaife, R. Allan, Recent seasonal asymmetric changes in the NAO (a marked summer decline and increased winter variability) and associated changes in the AO and Greenland Blocking Index. *Int. J. Climatol.* **35**, 2540–2554 (2015).

17. A. C. Bayliss, R. C. Jones, "Peaks-over-threshold flood database: Summary statistics and seasonality. IH Report No. 121" (Institute of Hydrology, Wallingford, UK, 1993).

18. B. Ivančan-Picek, K. Horvath, N. Mahović, M. Gajić-Čapka, Forcing mechanisms of a heavy precipitation event in the southeastern Adriatic area. *Nat. Hazards*. **72**, 1231–1252 (2014).

19. E. Xoplaki, J. F. Gonzalez-Rouco, J. Luterbacher, H. Wanner, Wet season Mediterranean precipitation variability: influence of large-scale dynamics and trends. *Clim. Dynam.* **23**, 63–78 (2004).

20. S. Klaus, H. Kreibich, B. Merz, B. Kuhlmann, K. Schröter, Large-scale, seasonal flood risk analysis for agricultural crops in Germany. *Environ. Earth Sci.* **75**, 1–13 (2016).

21. T. P. Barnett, J. C. Adam, D. P. Lettenmaier, Potential impacts of a warming climate on water availability in snow-dominated regions. *Nature*. **438**, 303–309 (2005).

22. M. Mudelsee, M. Boerngen, G. Tetzlaff, U. Gruenewald, No upward trends in the occurrence of extreme floods in central Europe. *Nature*. **425** (2003).

23. J. Hall *et al.*, A European Flood Database: facilitating comprehensive flood research beyond administrative boundaries. *Proc. Int. Assoc. Hydrol. Sci.* **370**, 89–95 (2015).

24. J. Vogt *et al.*, "A pan-European River and Catchment Database" (2007).

25. M. Haylock *et al.*, A European daily high-resolution gridded data set of surface temperature and precipitation for 1950-2006. *J. Geophys. Res.* **113** (2008), doi:10.1029/2008JD010201.

26. H. van den Dool, J. Huang, Y. Fan, Performance and analysis of the constructed analogue method applied to US soil moisture over 1981-2001. *J. Geophys. Res.* **108** (2003),

doi:10.1029/2002JD003114.

27. K. V. Mardia, *Statistics of directional data* (Academic Press Inc. London, 1972).

28. K. V. Mardia, P. E. Jupp, in *Directional Statistics* (John Wiley & Sons, Inc., 2008; http://dx.doi.org/10.1002/9780470316979.ch6), pp. 93–118.

29. H. Theil, A Rank-invariant Method of Linear and Polynomial Regression Analysis, Part 1. *Proc. R. Neth. Acad. Sci.* **53**, 386–392 (1950).

30. P. H. Hiemstra, E. J. Pebesma, C. J. Twenhöfel, G. B. Heuvelink, Real-time automatic interpolation of ambient gamma dose rates from the Dutch radioactivity monitoring network. *Comput. Geosci.* **35**, 1711–1721 (2009).

31. D. R. Helsel, L. M. Frans, Regional Kendall Test for Trend. *Environ. Sci. Technol.* **40**, 4066–4073 (2006).

32. G. Blöschl, T. Nester, J. Komma, J. Parajka, R. Perdigão, The June 2013 flood in the Upper Danube basin, and comparisons with the 2002, 1954 and 1899 floods. *Hydrol. Earth Syst. Sc.* **17**, 5197–5212 (2013).

33. R Core Team*: A Language and Environment for Statistical Computing* (2016; https://www.R-project.org).

34. D. Sarkar, *Lattice: Multivariate Data Visualization with R* (Springer, New York, 2008; http://lmdvr.r-forge.r-project.org).

35. R. Bivand, N. Lewin-Koh, *maptools: Tools for Reading and Handling Spatial Objects* (2016; https://CRAN.R-project.org/package=maptools).

36. D. Pierce, *ncdf4: Interface to Unidata netCDF (Version 4 or Earlier) Format Data Files* (2015; https://CRAN.R-project.org/package=ncdf4).

37. H. Wickham, The split-apply-combine strategy for data analysis. *J. Stat. Softw.* **40**, 1–29 (2011).

38. R. J. Hijmans, *raster: Geographic Data Analysis and Modeling* (2016; https://CRAN.R-project.org/package=raster).

39. E. Neuwirth, *RColorBrewer: ColorBrewer Palettes* (2014; https://CRAN.R-project.org/package=RColorBrewer).

40. R. Bivand, T. Keitt, B. Rowlingson, *rgdal: Bindings for the Geospatial Data Abstraction Library* (2016; https://CRAN.R-project.org/package=rgdal).

41. A. South, rworldmap: a new R package for mapping global data. *The R Journal*. **3**, 35–43 (2011).

Acknowledgments:

We would like to acknowledge the support of the ERC Advanced Grant "FloodChange", Project No. 291152, the Austrian Science Funds FWF as part of the Doctoral Programme on Water Resource Systems (W1219-N22), the EU FP7 project SWITCH-ON (Grant No 603587) and the Russian Science Foundation (Project No. 14-17-00155). The authors also acknowledge the involvement in the data screening process of C. Álvaro Díaz, I. Borzì (Sicily, Italy), E. Diamantini, K. Jeneiová, M. Kupfersberger, and S. Mallucci during their stays at the Vienna University of Technology. We also thank L. Gaál and D. Rosbjerg for contacting Finish and Danish data holders respectively and A. Christofides for pointing us to the Greek data source, B. Renard (France), T. Kiss (Hungary), W. Rigott (South Tyrol, Italy), G. Lindström (Sweden) and P. Burlando (Switzerland) for assistance in preparing and/or providing data or metadata from their respective regions, and B. Lüthi and Y. Hundecha for preparing supporting data to cross-check the results that are not part of the paper.

The flood date data used in this paper can be downloaded from http://www.hydro.tuwien.ac.at/fileadmin/mediapool-hydro/Downloads/Data.zip. The precipitation and temperature data can be downloaded from http://www.ecad.eu/download/ensembles/ensembles.php. The soil moisture data can be downloaded from http://www.esrl.noaa.gov/psd.

Supplementary Materials:

Materials and Methods

Supplementary Text

Figures S1 to S5

Tables S1 and S2

References (*23-41*)

Supplementary Materials for

Changing climate shifts timing of European floods

Günter Blöschl, Julia Hall, Juraj Parajka, Rui A. P. Perdigão, Bruno Merz, Berit Arheimer, Giuseppe T. Aronica, Ardian Bilibashi, Ognjen Bonacci, Marco Borga, Ivan Čanjevac, Attilio Castellarin, Giovanni B. Chirico, Pierluigi Claps, Károly Fiala, Natalia Frolova, Liudmyla Gorbachova, Ali Gül, Jamie Hannaford, Shaun Harrigan, Maria Kireeva, Andrea Kiss, Thomas R. Kjeldsen, Silvia Kohnová, Jarkko J. Koskela, Ondrej Ledvinka, Neil Macdonald, Maria Mavrova-Guirguinova, Luis Mediero, Ralf Merz, Peter Molnar, Alberto Montanari, Conor Murphy, Marzena Osuch, Valeryia Ovcharuk, Ivan Radevski, Magdalena Rogger, José L. Salinas, Eric Sauquet, Mojca Šraj, Jan Szolgay, Alberto Viglione, Elena Volpi, Donna Wilson, Klodian Zaimi, and Nenad Živković

correspondence to: bloeschl@hydro.tuwien.ac.at

This PDF file includes:

Materials and Methods

Data Sets

The hydrological data were obtained from a newly created European Flood Database (23) containing observations from 38 European countries for the period 1960 to 2010. The hydrological data used in this study consist of time series from 64 data holders/sources, which are listed in Table S1. The database of the flood dates can be downloaded from http://www.hydro.tuwien.ac.at/fileadmin/mediapool-hydro/Downloads/Data.zip

The database contains the date of the largest peak discharge or highest water level in each calendar year of the observed record (daily mean or instantaneous discharge) for each station. The dates of the maximum annual floods rather than those of multiple floods within a year are analyzed for two reasons. First, the climatological average of the flood timing over a decade or a number of decades can be more meaningfully defined if only a single flood per year is considered. Second, due to data licensing issues, for some areas, only the annual maxima were available.

Analyzing the dates of the floods provides deeper insights into the processes driving change than analyzing flood magnitudes alone. In addition, the date can be identified equally well from discharge and water level data which increases the temporal and spatial coverage. Finally, for some stations only the dates were available.

Stations located within the region bounded by the latitudes 34° N - 71° N and the longitudes 22° W - 52° E, with catchment areas between 5 and 100,000 km² and with more than 10 years of data during the study period were considered here. Although the data could be stratified into smaller and larger catchments, we collectively examined catchments of all areas to maintain spatial coverage and sample size. Stratifying the stations by catchment area did not change the large-scale patterns obtained in the analysis. Catchments that were reported by the data providers to have experienced strong human modifications that could affect the timing of floods were excluded. A few stations may still be affected by human modifications, but will have little impact on the overall result since the focus is on large-scale patterns of change. To account for the uneven spatial distribution of the hydrometric stations included in the database, in areas with high station densities such as Austria, Germany, and Switzerland, only stations with at least 49 years of data in the analysis period were included. This screening resulted in a set of 4262 stations (Fig. S1A, circles) with a median catchment size of 403 km². The elevation map plotted in the background of Fig. S1 was obtained from: https://www.eea.europa.eu/data-and-maps/data/digital-elevation-model-of-europe/.

The data from these stations were used for estimating the average timing of the annual flood peaks (Fig. 3). For estimating the change in the flood timing (Fig. 1 and 2), stations with at least 35 years of data during the analysis period (70% completeness) were considered, which resulted in 3298 stations (Fig. 1B, full circles) with a median catchment size of 420 km².

For each hydrometric station, the contributing catchment boundary was derived from the CCM River and Catchment Database (24) (http://www.bafg.de/GRDC/EN/01_GRDC/13_dtbse/database_node.html). The river network shown in the Figures is also taken from this database. Daily gridded precipitation and mean surface temperature data from the E-OBS data set (Version 14.0) (25) for the

period 1960-2010 were used (http://www.ecad.eu/download/ensembles/ensembles.php). The data consist of interpolated ground-based observations from stations with spatial resolutions of 0.5° x 0.5° and 0.25° x 0.25°. Monthly gridded soil moisture data from the CPC Soil Moisture data set (26) for the period 1960-2010 was analyzed (http://www.esrl.noaa.gov/psd). The data are model-calculated monthly averaged soil moisture water height equivalents with a spatial resolution of 0.5°.

Analysis Method

As a first step, we calculated for each station the average day within a year on which floods have occurred during the observation period. To account for the fact that floods can occur throughout the year, all calculations were performed using circular statistics (17, 27). Only those stations for which the null hypothesis of circular uniformity (Kuiper's test (28)) was rejected (significance level, α=0.1) were retained. This resulted in 4062 stations used in the analysis of the average timing, and 3184 stations for the trend analysis. Circular non-uniformity is considered necessary for a meaningful application of circular trend analysis.

The date of occurrence D_i of a flood in year i was converted into an angular value θ_i by

$$\theta_i = D_i \cdot \frac{2\pi}{m_i} \qquad 0 \le \theta_i \le 2\pi \tag{1}$$

where $D_i = 1$ corresponds to January 1 and $D_i = m_i$ to December 31, and where m_i is the number of days in that year. The average date of occurrence $\overline{D}$ of a flood at a station is defined as (17, 27):

$$\overline{D} = \begin{cases} \tan^{-1}\left(\frac{\bar{y}}{\bar{x}}\right) \cdot \frac{\overline{m}}{2\pi} & \bar{x} > 0,\ \bar{y} \ge 0 \\ \tan^{-1}\left(\frac{\bar{y}}{\bar{x}}\right) \cdot \frac{\overline{m}}{2\pi} + \pi & \bar{x} \le 0 \\ \tan^{-1}\left(\frac{\bar{y}}{\bar{x}}\right) \cdot \frac{\overline{m}}{2\pi} + 2\pi & \bar{x} > 0, \bar{y} < 0, \end{cases} \tag{2}$$

with

$$\bar{x} = \frac{1}{n}\sum_{i=1}^{n} \cos(\theta_i) \tag{3}$$

$$\bar{y} = \frac{1}{n}\sum_{i=1}^{n} \sin(\theta_i) \tag{4}$$

$$\overline{m} = \frac{1}{n}\sum_{i=1}^{n} m_i \tag{5}$$

where $\bar{x}$ and $\bar{y}$ are the cosine and sine components of the average date, respectively, $\bar{m}$ is the average number of days per year (365.25), and n is the total number of flood peaks at that station. The concentration R of the date of occurrence around the average date is

$$R = \sqrt{\bar{x}^2 + \bar{y}^2} \quad 0 \le R \le 1 \tag{6}$$

which ranges from $R = 0$ (no concentration, i.e. floods are widely dispersed throughout the year) to $R = 1$ (all floods at a station occur on the same day of the year).

As a second step, we estimated the trend in the timing by the adjusted Theil-Sen slope estimator (11, 29). This non-parametric estimator was chosen for its robustness and insensitivity to missing values and outliers. The trend estimator β is the median of the difference of dates over all possible pairs of years (i and j) within the time series,

$$\beta = \text{median}\left(\frac{D_j - D_i + k)}{j - i}\right) \text{ with } k = \begin{cases} -\bar{m} \text{ if } D_j - D_i > \bar{m}/2 \\ \bar{m} \text{ if } D_j - D_i < -\bar{m}/2 \\ 0 \text{ otherwise} \end{cases} \tag{7}$$

where k makes the adjustment for the circular nature of the dates and β has units of days per year. The value of β is plotted at the respective station location in Fig. S2. To identify large-scale spatial patterns within Europe, β was spatially interpolated using the *autoKrige* function (automatic kriging) within the R *automap* package (30), which automatically fits a variogram to the spatial data. The derived trend patterns are plotted in Fig. 1 and in the background of Fig. S2.

Third, we estimated the long-term evolution in flood timing with a centered 10-year moving average filter using Equations 2-6 (with n=10) to reduce the short-term year-to-year variability and sharpen the focus on long-term, decadal fluctuations. The periods 1960-1965 and 2005-2010 are shown in lighter colors in Fig. 2, as less than 10 years were available for calculating the average. We pooled these filtered series within sub-regions or hotspots that were selected based on their similarity, within a rectangular sub-region, of the average flood timing and its trends (Fig. S1). Names of the sub-regions are only indicative for a region and do not exactly correspond to any exactly defined geographic area. The series of flood timing within each hotspot were tested for evidence of a significant regionally consistent trend, using the Regional Mann-Kendall test (31). All regional trends were statistically significant at the α=0.05 level (Table S2). For each hotspot, the median timing for each year was calculated based on the data from each station within the hotspot. A 10-year moving average filter was then applied to the annual median timing to obtain the longer-term evolution of the time series within each hotspot (solid lines in Fig. 2). Additionally, we estimated the long-term evolution of the circular standard deviation σ,

$$\sigma = \sqrt{-2\ln(R)} \tag{8}$$

as a measure of the spread of flood occurrence within the year across all stations in the hotspot, and plotted σ as the widths of the bands in Fig. 2.

To investigate rain-induced effects on flood timing we identified for each grid point of the E-OBS dataset the 7-day period with the maximum precipitation in any calendar year (with at least 70% of the annual data available). We assigned the midpoint of the period as the date of the 7-day maximum precipitation, and repeated all timing and change analyses analogously to the floods described above (Fig. S3). Seven days are representative of flood generation in large catchments (32). In smaller catchments, shorter rainstorms (e.g. 1 or 3 days) may be more relevant. The average timing of the 1-day and 3-day maximum precipitation in Europe based on the E-OBS data set is very similar to the average timing of the 7-day maximum precipitation (Circular Pearson correlation coefficient r=0.91 and r=0.95, respectively), therefore we consider the 7-day maximum precipitation to be also representative for smaller catchments.

To understand the effect of snow processes on the flood timing we introduced a snowmelt-timing indicator as the first full seven days in a year when surface air temperatures exceeded 0° C. We only included those grid points at which such a date could be identified meaningfully in at least 70% of the years analyzed, i.e. where the 7-day temperatures were below 0° C before they started to rise in spring. The snowmelt-timing indicator is considered a proxy for both the snowmelt season and the transition from snowfall to rainfall. All timing and change analyses (Eq. 1 to Eq. 8) were repeated for maximum precipitation and the snowmelt indicator (Fig. S4).

When soil moisture is high, even small rainstorms may produce floods. To understand the effect of high soil moisture on floods, we identified for each grid point of the CPC Soil Moisture dataset the month of the highest soil moisture. We assigned the midpoint of the month as the date of maximum soil moisture and repeated all timing and change analyses (Eq. 1 to Eq. 8) (Fig. S5).

Only the data of grid points for which the null hypothesis of circular uniformity could be rejected (α=0.1) were used. For clarity of the visual presentation, Fig. S3A to S5A show only every other grid point. In the hotspot analyses (Fig. 2), the maximum precipitation, snowmelt indicator and maximum soil moisture data series were first extracted based on their location within the catchment boundaries and then aggregated for each hotspot.

All the data analysis mentioned above was performed in R (33) using the supporting packages *lattice* (34), *maptools* (35), *ncdf4*(36), *plyr* (37), *raster* (38), *RColorBrewer* (39), *rgdal* (40) and *rworldmap* (41).

Supplementary Text

Author Contributions

G.B. and J.H. designed the study and wrote the first draft of the paper.
G.B. initiated the study.
J.H. collated the database with the help of most of the co-authors, and conducted the analyses.
J.P. compiled the catchment boundaries and assisted in drafting the paper.
R.P. and B.M interpreted the results in the context of underlying geophysical mechanisms.
B.A, P.M and E.S provided additional data to crosscheck the results of this study.
All authors interpreted results, and contributed to framing and revising the paper.

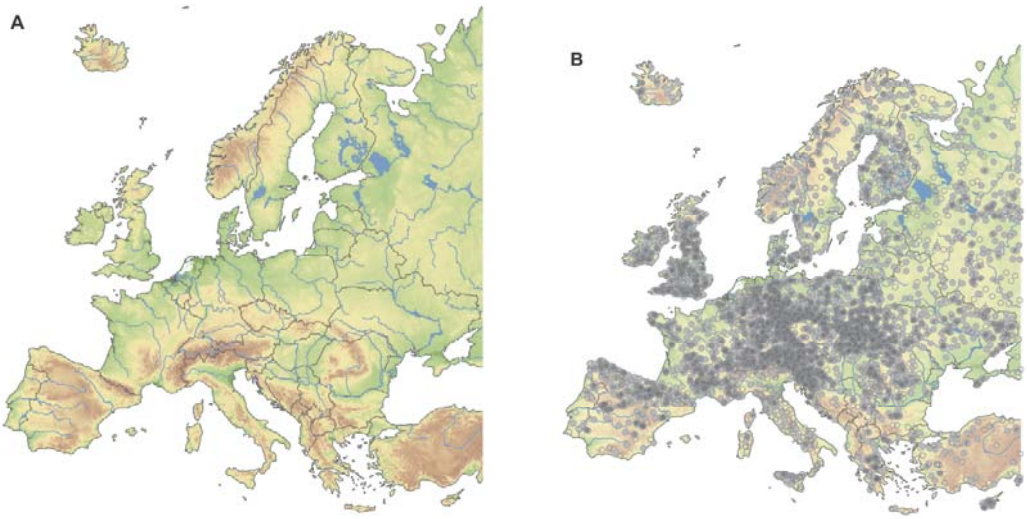

Fig. S1
Map of European study area, elevation, main rivers and lakes **(A)**, and location of the hydrometric stations analyzed **(B)**. Open and full circles indicate stations used for estimating the average flood timing ≥ 10 years of data, n=4262), full circles indicate stations used for estimating the change in flood timing (≥ 35 years of data, n=3298).

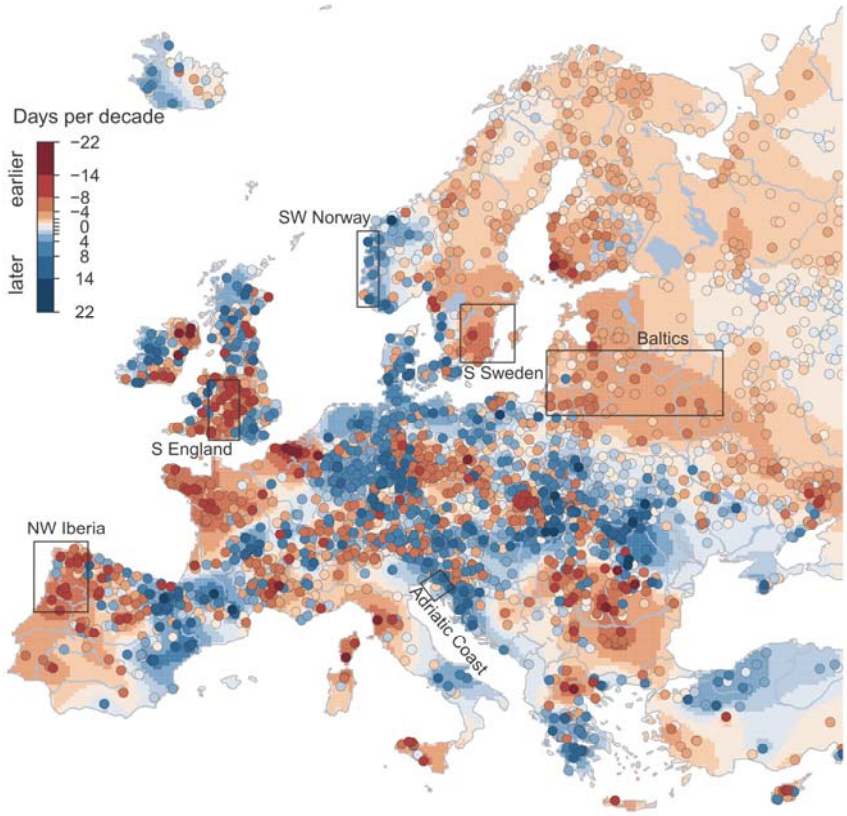

Fig. S2

Observed trends in flood timing 1960-2010, at individual hydrometric stations (points, n=3184) and interpolated trends (background pattern). Rectangles show selected sub-regions that were subject to a detailed regional analysis (Fig. 2).

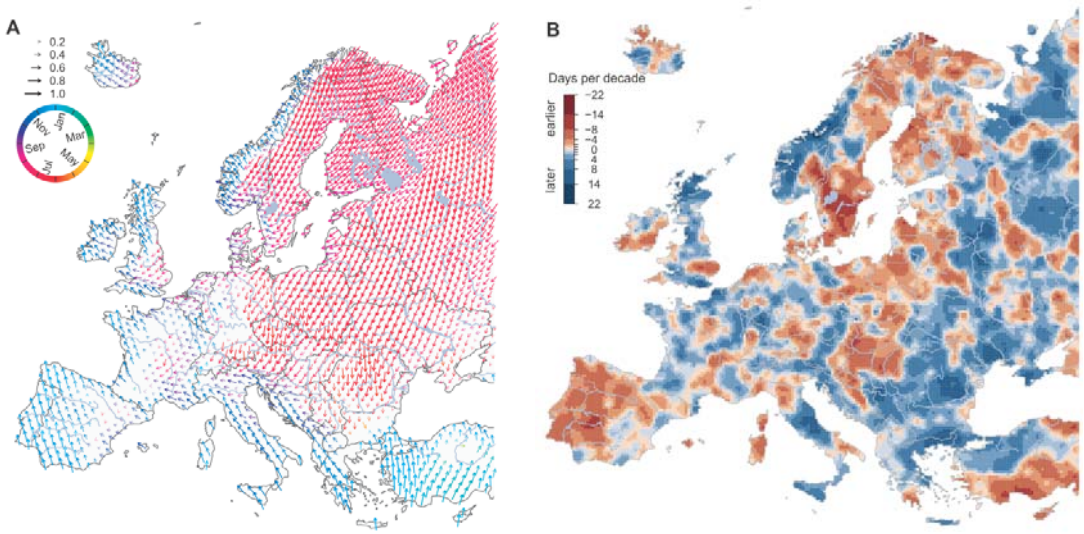

Fig. S3
7-day maximum precipitation (1960-2010). Average timing (color and direction of arrows) and concentration of timing within a year, R (length of arrows) (A), trend in timing; red indicates earlier precipitation, blue later precipitation (days per decade) (B).

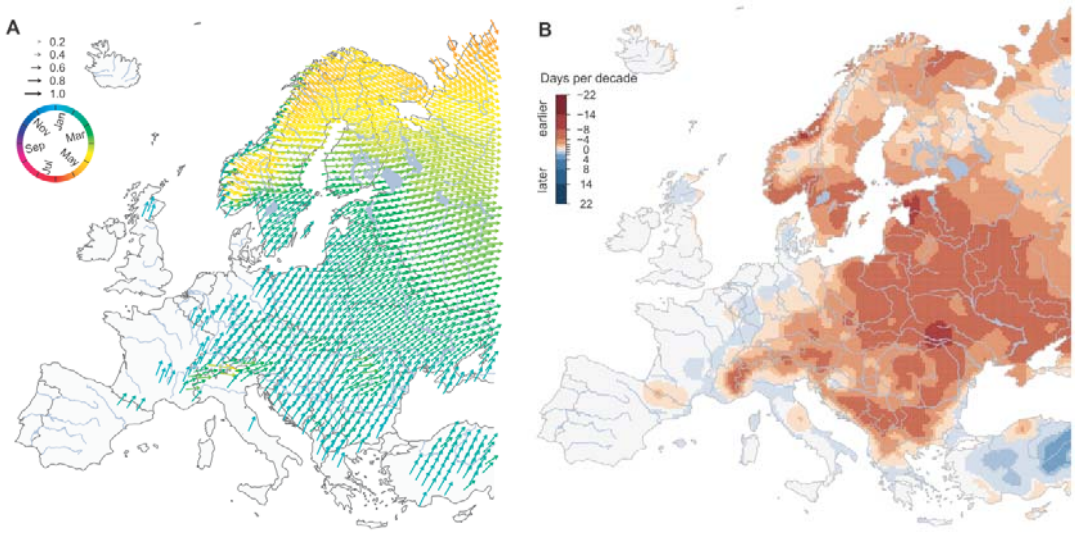

Fig. S4
Snowmelt indicator (1960-2010), first 7-days of the year with air temperature above 0° C. Average timing (color and direction of arrows) and concentration of timing within a year, R (length of arrows) (A), trend in timing; red indicates earlier snowmelt indicator, blue later snowmelt indicator (days per decade) (B).

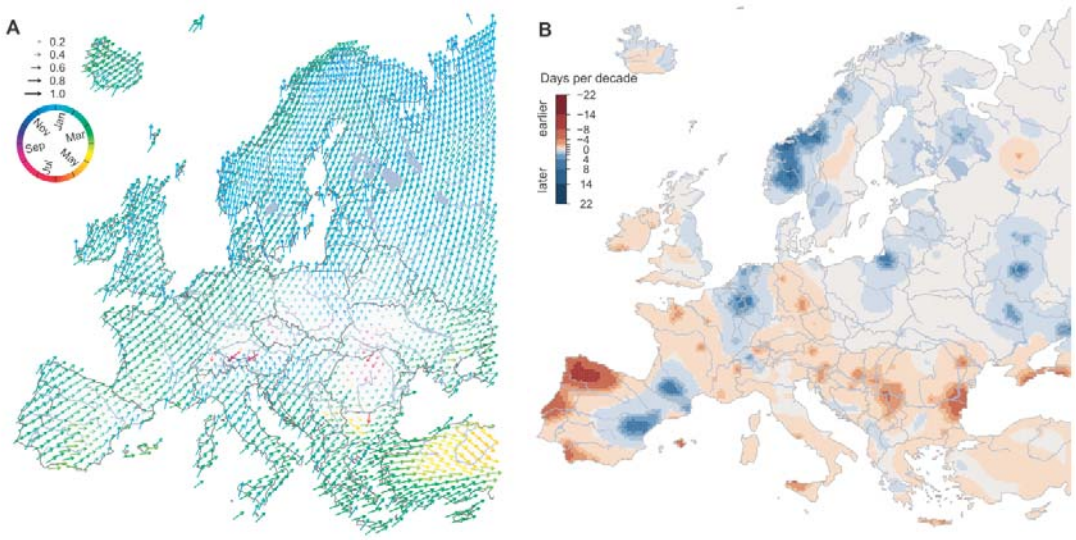

Fig. S5
Annual maximum monthly soil moisture (1960-2010). Average timing (color and direction of arrows) and concentration of timing within a year, R (length of arrows) (A), trend in timing; red indicates earlier soil moisture, blue later soil moisture (days per decade) (B).

Table S1.

Data Sources contained in the European Flood Research Database

Country/Project	Data Holder/Source/Project information
Albania	National Hydro-Meteorological Service Albania, Institute of GeoSciences, Energy, Water and Environment (IGEWE)
Austria	Hydrographic Services of Austria (HZB), Austrian Federal Ministry of Agriculture, Forestry, Environment and Water Management
Bosnia and Herzegovina	Hydrological Yearbooks of the former Republic of Yugoslavia
Bulgaria	Hydrological Yearbooks of the Rivers in Bulgaria, National Institute of Meteorology and Hydrology
Croatia	Meteorological and Hydrological Service of Croatia (DHMZ)
Czechia	Czech Hydrometeorological Institute
Denmark	Freshwater Scientific Data Centre, Danish Centre for Environment and Energy (DCE)
Estonia	Estonian Environment Agency (KAUR)
EWA	European Water Archive (EWA)
Finland	Finnish Environment Institute, Open information/Hydrology/Discharge(SYKE)
France	HYDRO database, French Ministry of Ecology, Sustainable Development and Energy
Germany	Federal Waterways and Shipping Administration (WSV)
Germany, Bavaria	Bavarian Environment Agency (LfU)
Germany, Brandenburg	Brandenburg State Office of Environment, Health and Consumer Protection (LUGV)
Germany, Hesse	Hessian Agency for Nature Conservation, Environment and Geology (HLNUG)
Germany, Lower Saxony	Lower Saxony Water Management, Coastal Defense and Nature Conservation Agency (NLWKN)
Germany, Mecklenburg-Vorpommern	State Office of Environment, Nature Protection and Geology of Mecklenburg-Vorpommern (LUNG)
Germany, North Rhine-Westphalia	North Rhine-Westphalia State Agency for Nature, Environment and Consumer Protection (LANUV),
Germany, Rhineland-Palatinate	State Office for the Environment (LfU), Rhineland-Palatinate
Germany, Saarland	The Saarland State Office for Environmental and Labor Protection (LUA)
Germany, Saxony	Saxon State Agency for Environment, Agriculture and Geology (LfULG)
Germany, Saxony-Anhalt	State Agency for Flood Defense and Water Management of Saxony-Anhalt (LHW)
Germany, Schleswig-Holstein	Schleswig-Holstein Agency for Coastal Defense, National Park and Marine Conservation (ACNM-SH)
Germany, Thuringia	Thuringian State Institute for the Environment and Geology (TLUG)
GRDC	The Global Runoff Data Centre, Koblenz, Germany

Greece	Hydroscope- Ministry for the Environment, Energy and Climate Change - Special Secretariat for Water
Hungary	General Directorate of Water Management, Hungary
Hungary	Lower Tisza District Water Directorate
HYDRATE	HYDRATE Project data base: Hydrometeorological Data Resources and Technology for Effective Flash Flood Forecasting
Ireland	Irish Environmental Protection Agency (EPA)
Ireland	Office of Public Works (OPW)
Italy	Former National Hydrographic Service (SIMN)
Italy	The Italian National Institute for Environmental Protection and Research (ISPRA)
Italy	National Research Council (CNR)
Italy, Bolzano, South Tyrol Region	Hydrological Services, Autonomous Province of Bozen/Bolzano - South Tyrol
Italy, Emilia-Romagna Region	Regional Agency for the Environmental Protection (ARPA), Emilia–Romagna
Italy, Lazio & Umbria	Bencivenga M., Calenda G. and Mancini C.P., 2001.
Italy, Piedmont Region	Italian National Agency for Electricity (ENEL)
Italy, Piedmont Region	Research Institute for Hydro-Geologic Protection (IRPI)
Italy, Piedmont Region	Regional Agency for the Environmental Protection (ARPA), Piemonte
Italy, Po Region	Basin Authority of the Po River
Italy, Sicily Region	Water Observatory - Sicily Region
Italy, Trentino Region	Civil Protection Department, Autonomous Province of Trento
Italy, Tuscany Region	Regional Functional Center of Meteo-Hydrological Monitoring, Tuscany
Italy, Veneto Region	Regional Agency for the Environmental Protection (ARPA), Veneto
Latvia	Latvian Environment, Geology and Meteorology Centre
Lithuania	Lithuanian Hydrometeorological Service under the Misnstry of Environment
Netherlands	Dutch Ministry of Infrastructure and the Environment - Rijkswaterstaat
Norway	Database Hydra II; Norwegian Water Resources and Energy Directorate (NVE)
Poland	Institute of Meteorology and Water Management National Research Institute (IMGW-PIB)
Portugal	Portuguese Environmental Agency National Information System for Water Resources of Portugal (SNIRH)
Republic of Macedonia	National Hydrometeorological Service, Republic of Macedonia
Russia	Ministry of Natural Resources and Ecology of the Russian Federation
Russia	State Water Cadastre, State Hydrological Institute, Lomonosov Moscow State University
Russia	AIS GMVO, Russian Federal Agency for Water Resources
Serbia	Republic Hydrometeorological Service of Serbia (RHSS)
Slovakia	Slovak Hydrometeorological Institute, Bratislava (SHMI)
Slovenia	Slovenian Environment Agency (ARSO)

Spain	Centre for Hydrographic Studies of CEDEX, Ministry of Agriculture, Food and Environment, Spain
Sweden	Swedish Meteorological and Hydrological Institute (SMHI)
Switzerland	Federal Office for the Environment (BAFU)
Turkey	General Directorate of Electrical Power Resources Survey and Development Administration (EIE), Turkey
Ukraine	Hydrological Department, Ukrainian Hydrometeorological Institute (UHMI)
Ukraine	Hydrometeorological Institute, Odessa State Environmental University (OSENU)
United Kingdom	UK National River Flow Archive (NRFA)

Table S2.

Changes in timing for selected hotspots. Trend slopes are in days per decade. Negative signs indicate earlier flood timing, positive values later flood timing. The significance level of the regional trends is given according to the Regional Mann-Kendall test with significance level alpha (α).

Hotspot Name	No. of Stations	Maximum Slope	Minimum Slope	Regional Change slope	Regionally Significant
S Sweden	12	-1.58	-10.01	-4.84	α=0.01
Baltics	43	6.52	-7.46	-3.44	α=0.01
SW Norway	6	14.13	-2.30	7.91	α=0.01
S England	49	12.34	-112.3	-4.65	α=0.01
NW Iberia	25	2.90	-12.82	-6.67	α=0.01
Adriatic Coast	19	9.92	-1.73	3.28	α=0.05

References:

23. J. Hall *et al.*, A European Flood Database: facilitating comprehensive flood research beyond administrative boundaries. *Proc. Int. Assoc. Hydrol. Sci.* **370**, 89–95 (2015).

24. J. Vogt *et al.*, "A pan-European River and Catchment Database" (2007).

25. M. Haylock *et al.*, A European daily high-resolution gridded data set of surface temperature and precipitation for 1950-2006. *J. Geophys. Res.* **113** (2008), doi:10.1029/2008JD010201.

26. H. van den Dool, J. Huang, Y. Fan, Performance and analysis of the constructed analogue method applied to US soil moisture over 1981-2001. *J. Geophys. Res.* **108** (2003), doi:10.1029/2002JD003114.

27. K. V. Mardia, *Statistics of directional data* (Academic Press Inc. London, 1972).

28. K. V. Mardia, P. E. Jupp, in *Directional Statistics* (John Wiley & Sons, Inc., 2008; http://dx.doi.org/10.1002/9780470316979.ch6), pp. 93–118.

29. H. Theil, A Rank-invariant Method of Linear and Polynomial Regression Analysis, Part 1. *Proc. R. Neth. Acad. Sci.* **53**, 386–392 (1950).

30. P. H. Hiemstra, E. J. Pebesma, C. J. Twenhöfel, G. B. Heuvelink, Real-time automatic interpolation of ambient gamma dose rates from the Dutch radioactivity monitoring network. *Comput. Geosci.* **35**, 1711–1721 (2009).

31. D. R. Helsel, L. M. Frans, Regional Kendall Test for Trend. *Environ. Sci. Technol.* **40**, 4066–4073 (2006).

32. G. Blöschl, T. Nester, J. Komma, J. Parajka, R. Perdigão, The June 2013 flood in the Upper Danube basin, and comparisons with the 2002, 1954 and 1899 floods. *Hydrol. Earth Syst. Sc.* **17**, 5197–5212 (2013).

33. R Core Team*: A Language and Environment for Statistical Computing* (2016; https://www.R-project.org).

34. D. Sarkar, *Lattice: Multivariate Data Visualization with R* (Springer, New York, 2008; http://lmdvr.r-forge.r-project.org).

35. R. Bivand, N. Lewin-Koh, *maptools: Tools for Reading and Handling Spatial Objects* (2016; https://CRAN.R-project.org/package=maptools).

36. D. Pierce, *ncdf4: Interface to Unidata netCDF (Version 4 or Earlier) Format Data Files* (2015; https://CRAN.R-project.org/package=ncdf4).

37. H. Wickham, The split-apply-combine strategy for data analysis. *J. Stat. Softw.* **40**, 1–29 (2011).

38. R. J. Hijmans, *raster: Geographic Data Analysis and Modeling* (2016; https://CRAN.R-project.org/package=raster).

39. E. Neuwirth, *RColorBrewer: ColorBrewer Palettes* (2014; https://CRAN.R-project.org/package=RColorBrewer).

40. R. Bivand, T. Keitt, B. Rowlingson, *rgdal: Bindings for the Geospatial Data Abstraction Library* (2016; https://CRAN.R-project.org/package=rgdal).

41. A. South, rworldmap: a new R package for mapping global data. *The R Journal*. **3**, 35–43 (2011).